NASA Technical Paper 1003

The NASA Ames Research Center One- and Two-Dimensional Stratospheric Models

Part II: The Two-Dimensional Model

R. C. Whitten, W. J. Borucki, V. R. Watson,
T. Shimazaki, H. T. Woodward, C. A. Riegel,
L. A. Capone, and T. Becker

SEPTEMBER 1977

NASA

NASA Technical Paper 1003

The NASA Ames Research Center One- and Two-Dimensional Stratospheric Models

Part II: The Two-Dimensional Model

R. C. Whitten, W. J. Borucki, V. R. Watson,
T. Shimazaki, and H. T. Woodward
Ames Research Center
Moffett Field, California

C. A. Riegel and L. A. Capone
San Jose State University
San Jose, California

T. Becker
Informatics, Inc.
Palo Alto, California

National Aeronautics
and Space Administration

**Scientific and Technical
Information Office**

1977

THE NASA AMES RESEARCH CENTER ONE- AND TWO-DIMENSIONAL STRATOSPHERIC MODELS

PART II: THE TWO-DIMENSIONAL MODEL

R. C. Whitten,* W. J. Borucki,* V. R. Watson,* T. Shimazaki,*
H. T. Woodward,* C. A. Riegel,† L. A. Capone,† and T. Becker‡

SUMMARY

The Ames two-dimensional model of stratospheric trace constituents is presented in detail. The derivation of pertinent transport parameters and the numerical solution of the species continuity equations, including a technique for treating the "stiff" differential equations that represent the chemical kinetic terms, and appropriate methods for simulating the diurnal variations of the solar zenith angle and species concentrations are discussed. Predicted distributions of tracer constituents (ozone, carbon 14, nitric acid) are compared with observed distributions.

INTRODUCTION

In this paper we discuss the two-dimensional atmospheric model developed at Ames Research Center: its geometry, techniques for solving the associated photochemical continuity equations, and the derivation and inclusion of appropriate transport parameters. Two-dimensional models are justified because: (1) zonal spreading and mixing of trace constituents is much more rapid than is meridional spreading and mixing, thus validating the assumption of zonal symmetry for most applications; (2) meridional bulk velocity and eddy diffusivity fields can be constructed by choosing them such that distributions of several tracers with different "chemistries" are satisfactorily simulated while the fields themselves are in rough agreement with observed winds and their variances; and (3) reasonably complete sets of chemical species and reactions can be accommodated without the excessive demands on computer time that would be required by three-dimensional models. Because this article is intended to emphasize the mechanics and numerical methods used rather than predictions of trace gas distributions and the effects of perturbations thereof on the Earth's ozone shield, we restrict our discussion accordingly.

To complement this review we refer the reader to our recent publication (ref. 1) on the effects of supersonic transport emissions on the ozone layer; additional papers describing results for trace gas distributions in the

*Ames Research Center
†Dept. of Meteorology, San Jose State Univ.
‡Informatics, Inc.

ambient atmosphere and for effects on atmospheric ozone of chlorofluoromethanes and of HCl emitted by space shuttle launch vehicles are now being prepared. We emphasize that our two-dimensional model is under continuing development and has not yet reached the same state of maturity as the one-dimensional model of Turco and Whitten (ref. 2). The geometry of the model is shown in figure 1.

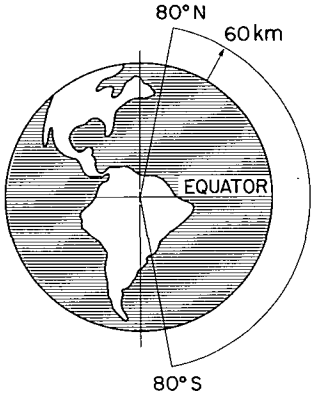

Figure 1.- Model geometry.

The chemistry employed in this model is a somewhat simplified version of that used in our one-dimensional model studies (e.g., ref. 2). Because of the computational time demands of a two-dimensional model, it is necessary to include only that set of species and chemical reactions that is essential to realistic simulation of species distributions. Hence, our chemical set is smaller than that in the one-dimensional model (ref. 2). In arriving at the chemical reaction set in the two-dimensional model we used simulations from the one-dimensional model as a guide, ignoring those reactions that have very little effect on production and loss rates of the constituents. At each time step, the model calculates the concentrations of O_3, $O(^3P)$, $O(^1D)$, N, NO_2, NO, NO_3, N_2O, N_2O_5, HNO_3, HNO_2, H_2O_2, HO_2, OH, H, Cl, ClO, HCl, $CFCl_3$, and CF_2Cl_2. The profiles of N_2, O_2, CO_2, CO, CH_4, and H_2O are held fixed (at experimentally determined values) during the calculation. However, the program is now being modified to allow CH_4 and CO, and stratospheric H_2O to vary during the computations.

SPECIES CONTINUITY EQUATIONS

The model is based on the governing equations for trace constituents:

$$\frac{\partial n_i}{\partial t} + \underset{\sim}{\nabla} \cdot \underset{\sim}{\Phi}_i = P_i - L_i \tag{1}$$

with the flux, Φ_i, expressed as the sum of a term that represents large scale mean meridional bulk motion and a term that represents smaller scale mixing caused by "eddy" motions

$$\underset{\sim}{\Phi}_i = \underset{\sim}{v} n_i - \underset{\sim}{K}_e \cdot \left[\underset{\sim}{\nabla} n_i + \left(\frac{1}{H} + \frac{1}{T} \frac{dT}{dz} \right) n_i \hat{e}_z \right] \tag{2}$$

Here, n_i and $\underset{\sim}{\Phi}_i$ are the concentration and flux, respectively, of the ith constituent; P_i and L_i are the respective chemical production and loss terms;

H and T are the atmospheric scale height and temperature; $\hat{e}_z$ is a vertical unit vector; v is the atmospheric bulk velocity; and K_e is the eddy diffusivity tensor for which the symmetry is assumed. The quantities H and T are related by the equality

$$H = k_B \frac{T}{\bar{m}g} \tag{3}$$

in which k_B is Boltzmann's constant, g is gravitational acceleration, and $\bar{m}$ is the mean molecular mass in the well-mixed atmosphere. The temperature, T, which is a function of season and latitude as well as altitude, is taken from Oort and Rasmussen (ref. 3) for altitudes below 20 km and from Nastrom and Belmont (ref. 4) for higher altitudes. The two-dimensional "del" operator is represented in the meridional plane of a sphere by

$$\underset{\sim}{\nabla} = \frac{\hat{e}_\theta}{R \cos \theta} \frac{\partial}{\partial \theta} \cos \theta + \hat{e}_z \frac{\partial}{\partial z} \tag{4}$$

where θ is the latitude, $\hat{e}_\theta$ is a tangential unit vector, and R is the radius of Earth.

The term $P_i - L_i$, which represents the net production rate of a species, can be written

$$\begin{aligned} Q_i &\equiv P_i - L_i \\ &= \sum_{j,k} \varepsilon_{ijk} k_{jk} n_j n_k \end{aligned} \tag{5}$$

where ε_{ijk} is ± 1, depending on whether the species is produced or destroyed, respectively, and k_{jk} is the rate coefficient for the reaction. If the process is photolytic, we have $n_j = 1$ and

$$k_{jk} = J_k \tag{6}$$

with J_k the photolysis rate.

Transport parameters are specified in the model for each season. They are of two types: bulk velocity, which represents large scale mean meridional motion, and "eddy diffusivity," which represents smaller scale motions. The parameters that we have adopted are physically reasonable and lead to satisfactory predictions of observed tracer distributions.

The mean meridional circulation is obtained by the kinematic method from the averaged equation of mass continuity, which states that

$$\frac{\partial \rho}{\partial t} + \underset{\sim}{\nabla} \cdot (\rho \underset{\sim}{V}) = 0 \tag{7}$$

where ρ is the atmospheric bulk density and $\underset{\sim}{V}$ is the large scale atmospheric velocity. With the assumption that the density field is in a steady state, the approximate form of this equation in spherical coordinates is

$$\frac{1}{R \cos \theta} \frac{\partial}{\partial \theta} (\bar{\rho}\bar{v} \cos \theta) + \frac{\partial}{\partial z} (\bar{\rho}\bar{w}) = 0 \tag{8}$$

where the overbar denotes an average with respect to time and longitude, and $\bar{v}$ and $\bar{w}$ are the mean meridional and vertical velocity components. Equation (8) implies the existence of a "stream function" ψ for the total flux such that

$$2\pi R\bar{\rho}\bar{v} \cos \theta = - \frac{\partial \psi}{\partial z} ; \quad 2\pi R\bar{\rho}\bar{w} \cos \theta = \frac{1}{R} \frac{\partial \psi}{\partial \theta} \tag{9}$$

If the distributions of $\bar{\rho}$ and $\bar{v}$ are known, the first of equations (9) can be integrated vertically to obtain ψ, and $\bar{w}$ can then be obtained from the second. The required boundary conditions on ψ are discussed below.

The density was obtained from the hydrostatic equation using temperature data presented by Oort and Rasmussen (ref. 3) for altitudes to 20 km; for higher altitudes mean (rocket) temperatures were used (ref. 4).

The $\bar{v}$ components were based on the observed data of Oort and Rasmussen (ref. 3) for altitudes to 20 km. These values were then extrapolated to the top of the model by imposition of a simple vertical profile that matched the 20-km value and satisfied the kinematic constraint that there be no net mass flux across any vertical latitude wall. In addition, a meridional behavior was imposed such that a three-cell circulation structure (80° N to 80° S) in the stratosphere and lower mesosphere resulted during the summer and winter seasons, and a four-cell structure in spring and fall. This should approximate the circulation patterns obtained by other investigators (e.g., Murgatroyd and Singleton, ref. 5; Vincent, ref. 6).

The first of equations (9) was then integrated vertically with the condition that $\psi = 0$ on all boundaries. Meridional wind speeds are generally less than 1 m sec^{-1}, except in the upper equatorial troposphere. Small mean meridional velocities are, of course, expected because they result from the (small) ageostrophic part of the circulation system. Vertical wind speeds attain maxima in excess of 4 mm sec^{-1} in the equatorial troposphere, but are usually less than 1 mm sec^{-1} except in the vicinity of cell boundaries. Stream functions for fall in the Northern Hemisphere are shown in figure 2.

The eddy fluxes are modeled by diffusion coefficients K_{yy}, K_{yz}, and K_{zz} (the local "y" axis is tangent to the meridian; i.e., $dy = Rd\theta$). Because the motivation for choosing the general shape of the K_{zz} profile is described in great detail in Turco and Whitten (ref. 2), we do not repeat it here. It is sufficient to note that the magnitude of K_{zz} in this model is generally somewhat smaller than that in a one-dimensional model because vertical transport in two-dimensional models is affected by large scale bulk motion ($\bar{w}$) as well as by eddy mixing. The values of K_{yy}, which is the horizontal analogue

of K_{zz}, are strongly latitude-dependent, but height-independent, as shown in figure 3; we note that it was not necessary to make K_{yy} height-dependent in order to match observed tracer distributions. The magnitude tends to be large at high latitudes in winter and spring when the wind shears arising from the polar vortex cause the formation of strong eddy motions. On the other hand, K_{yy} is smaller in the tropics where zonal flow and thus eddy formation are weaker. Our meridional variation of K_{yy} is different from that of Louis (ref. 7), who adopted larger K_{yy} at low latitude than at high latitudes; Louis's choice of K_{yy} does not yield the observed ozone distribution when chemistry is included in the model (see the results section).

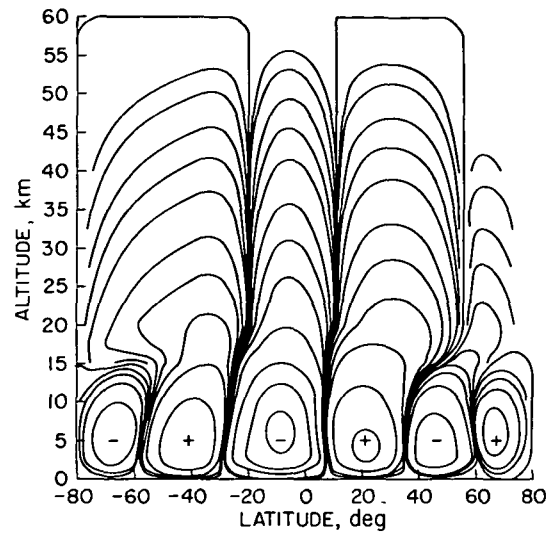

Figure 2.- Stream function; fall in the Northern Hemisphere.

The most interesting of the K_{ij}, however, is the "off-diagonal" K_{yz} because it leads to an apparent counter-gradient flux of ozone. It has been convincingly argued by Newell (ref. 8) that the "mixing surfaces" in the lower stratosphere slope more steeply toward the pole than do the surfaces of potential temperature. That is, parcels of ozone moving poleward in the lower stratosphere tend also to move farther downward in the transport region to altitudes where their destruction becomes less efficient. Hence we see a buildup of ozone column density at high latitudes. The reason for the difference in slope of the potential temperature and mixing surfaces lies in the effect of eddy motions in the lower atmosphere. In poleward moving air these motions tend to force the air parcels downward below the surfaces of potential temperature, the surfaces of natural movement in quiet stable air. One can in principle calculate the K_{ij} by computing the variances of observed winds over a long period of time. In practice, one can obtain only order-of-magnitude estimates in this way. Our K_{ij}, which are based on observed tracer distributions, are consistent with the order-of-magnitude estimates obtained

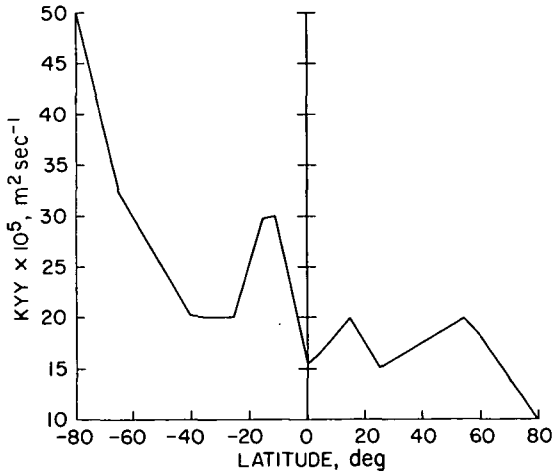

Figure 3.- K_{yy}; fall in the Northern Hemisphere. K_{yy} is independent of height in our model.

from wind variance calculations. In order to facilitate computation of the K_{ij}, we employ a suggestion by Brasseur[1] that they be expressed in the form

$$K_{ij} = \Theta_{ij}(\theta) Z_{ij}(z) \tag{10}$$

where Θ is a function of latitude alone and Z is a function of height alone (note that our $Z_{yy} = 1$). These functions are readily adjusted to yield K-fields that result in smooth distributions of trace constituents.

BOUNDARY CONDITIONS

End boundaries are taken at 80° S and 80° N because meridional fluxes are expected to be small at those latitudes. Hence, the end boundary conditions are taken to be zero flux of all constituents across the vertical boundaries. The upper boundary conditions are given by setting the fluxes equal to zero for all species. We have checked the upper boundary conditions (at 60 km) for the various species against results from a one-dimensional model that extended up to 120 km. It was found that the effect of choosing a mixing equilibrium condition at the upper boundary had very little effect on any of the constituents at altitudes below 50 km. The lower boundary condition used for all species except N_2O, CH_4, HNO_3, NO_2, O_3, HCl, H_2O_2 and the halocarbons, is chemical equilibrium because of their short lifetimes against chemical loss. Because HNO_3, HCl, and H_2O_2 are water soluble, their number densities are set equal to zero at the lower boundary. The number densities of CH_4, NO_2, and N_2O are fixed at 3.7×10^{13} cm^{-3}, 3×10^{9} cm^{-3}, and 7.5×10^{12} cm^{-3}, respectively, at the lower boundary, and that of O_3 is fixed at 6×10^{11} cm^{-3} (ref. 9) in order to conform to measured values. The boundary conditions for $CFCl_3$ and CF_2Cl_2 are time-variable fluxes that are set equal to the chlorofluorocarbon release rates (ref. 10).

NUMERICAL SOLUTION OF THE SPECIES CONTINUITY EQUATIONS

We now turn our attention to the numerical solution of the governing equations. The method of "time splitting" is used to facilitate the computation; that is, the chemistry and transport portions of the equations are in general solved at different time steps. The technique for the "chemistry" step is discussed first; the technique that applies to transport is described in following sections.

---

[1]Private communication from Brasseur, Institut d'Aéronomie Spatiale de Belgique, Brussels.

We avoid the instabilities associated with "stiffness"[2] by employing an approach that is closely related to the "families" method developed by Turco and Whitten (refs. 2, 11). We prefer the following technique to that of Turco and Whitten because in a two-dimensional model it appears to cause fewer difficulties at high latitudes where the solar illumination vanishes near the winter pole.

The chemical rate equations are solved using the following type of implicit technique. Equations (1) and (5) yield the finite difference form

$$\frac{n_i^{j+1} - n_i^j}{\Delta t} = Q_i^{j+1} \tag{11}$$

in which the superscript j indicates the index of the time step Δt. Equation (11) can be linearized by taking the first term in a Taylor series expansion about Q_i^j:

$$\frac{n_i^{j+1} - n_i^j}{\Delta t} = Q_i^j + \sum_{k=1}^{m} \frac{\partial Q_i^j}{\partial n_k} \left(n_k^{j+1} - n_k^j \right) \tag{12}$$

The m members of the set of mass conservation equations are thus coupled and require solution by inversion of a large matrix at each grid point. The 24 species in the Ames two-dimensional model are grouped into sets of closely coupled species that interchange rapidly (small time constants); but the species in a set are only weakly coupled to the species not contained in the set (large time constants). For example, a set containing the odd-oxygen species O_3, $O(^1D)$, and O need not contain NO_3, N_2O_5, HNO_3, HNO_2, N_2O, or H_2O_2. Because the computation time required for matrix inversion is roughly proportional to the square of the number of species, a careful segmentation into a number of smaller matrices substantially reduces the computer time required for solution. This method allows large time steps (about 1 day for most applications) to be taken even though the equations are very stiff. The technique is very efficient and yields results that agree well with those obtained with a linearized fully implicit method (ref. 1). Table 1 lists the various closely-coupled sets and their members.

The photodissociation coefficient J_i of the ith constituent at wavelength λ and height z is calculated from the expression

$$J_i(z,\lambda) = \varepsilon_i(\lambda)\sigma_i(\lambda)I_\infty(\lambda)e^{-\tau(\lambda,z)} \tag{13}$$

---

[2]A system of "stiff" coupled differential equations is characterized by time constants that span a large range of values. Use of large time steps does not permit the systems to respond to the small time constants. This characteristic can lead to computational instability unless special precautions, such as that described here, are taken.

TABLE 1.- THE SETS OF SPECIES

No.	Components
1	O_3, $O(^3P)$, $O(^1D)$, NO_2, Cl, ClO, HCl
2	OH, HO_2, H_2O_2, H, HNO_3, HNO_2
3	NO, NO_2, NO_3, N, N_2O_5, HNO_3, HNO_2

Note: Solution of the matrix equations must be in the order listed; for example, NO_x compounds (set no. 3) must be determined after the solution for set no. 2, *not* no. 1.

where σ_i is the absorption cross section of the ith constituent, I_∞ is the intensity of solar radiation (number of photons cm^{-2} sec^{-1} (unit $\lambda)^{-1}$ at the top of the atmosphere), $\varepsilon_i(\lambda)$ is the quantum yield, and τ is the optical depth given approximately by

$$\tau(\lambda,z) = \left[\sigma_{O_2}(\lambda)\int_z^\infty n_{O_2}\,dz + \sigma_{O_3}(\lambda)\int_z^\infty n_{O_3}\,dz + \sigma_{NO_2}(\lambda)\int_z^\infty n_{NO_2}\,dz\right]\sec\chi \tag{14}$$

for small solar zenith angle, χ. At larger χ a ray tracing routine is used to determine the physical path length. The optical depth is, of course, implicitly time-dependent through temporal changes in n_{O_3}, but for clarity we have omitted time (t) from the arguments. In order to calculate the integrated dissociation coefficient over a wavelength region (λ_0 to λ_T), we divide it into a number of intervals ($\lambda_0 - \lambda_1$, $\lambda_1 - \lambda_2$, . . ., $\lambda_n - \lambda_T$), which include the Schumann-Runge bands. Then the total photodissociation coefficient is calculated by

$$J_i(z) = \int_{\lambda_0}^{\lambda_T} J_i(\lambda,z)\,d\lambda$$

$$= \sum_{k=0}^{T-1}\int_{\lambda_k}^{\lambda_{k+1}} I_\infty(\lambda)\sigma_i(\lambda)\varepsilon_i(\lambda)\exp\left\{-\left[\tau_{O_2}(\lambda,z) + \tau_{O_3}(\lambda,z) + \tau_{NO_2}(\lambda,z)\right]\right\}d\lambda \tag{15}$$

Because σ_{O_2} and hence τ_{O_2} are very strong functions of λ in the Schumann-Runge band system (175-205 nm), special methods must be used in that spectral region. Hudson and Mahle (ref. 12) performed a line-by-line integration using theoretical line profiles for column densities N between 1×10^{17} cm^{-2} and 7×10^{24} cm^{-2} and for temperatures between 150 and 300 K. Interpolation constants were then found for 19 wavelength bands spanning the 175-205 nm spectral region for both the oxygen photolysis rate and the optical depth. Because the 5538 interpolation constants must be stored in memory, and because

interpolation is required to obtain a specific value of the photodissociation rate and optical depth, the Hudson-Mahle model is expensive to use.

In order to reduce the computational time Shimazaki and Ogawa (refs. 13 and 14) developed a modification of the Hudson and Mahle technique in which they derived polynomial formulas of the seventh degree for computing the integrals, which appear in equation (14), as functions of N:

$$\ell n\ I = \sum_{k=0}^{7} P_k (\ell n\ N)^k \tag{16}$$

The coefficients P_k are determined by a least squares best fit to the Hudson-Mahle results. The Ames two-dimensional model uses 6 equal intervals of 5 nm each in the Schumann-Runge bands and 51 intervals throughout the remainder of the solar spectrum. Shimazaki et al. (ref. 15) have carefully compared the J_i obtained in this way for all of the important stratospheric photodissociation processes, and found excellent agreement (within 10 percent) with the Hudson-Mahle approach.

Ideally, one would like to perform computations of the concentrations of stratospheric trace constituents that fully include the effects of diurnal variations. Unfortunately, the small time-steps required for a full diurnal simulation are as a rule much too expensive in terms of computer time requirements. Hence, we prefer to use some means of approximating the diurnal effects. Such a simulation will allow for change of the solar zenith angle during the day, absence of solar illumination during the night, and very substantial change in concentration of some of the constituents from day to night. The diurnally-averaged photodissociation rates are obtained by approximating the time integral of equation (15) (see Cogley and Borucki, ref. 16). The approximation considers the number of hours of daylight at each latitude and season, and matches various properties of the exponential integral and exponential functions.

Turco and Whitten (refs. 2, 17) have developed a method for averaging the species concentrations which simulates quite well the results obtained from a full diurnal calculation of the trace constituents. The most sensitive test of the technique is the calculation of the N_2O_5 abundance because of the slow build-up of N_2O_5 over many diurnal cycles. The results obtained with the Turco and Whitten method are within 20 percent of those obtained with a full diurnal calculation. In applying this averaging technique to the two-dimensional model, one must be sure to use it at *every* latitude because of the latitudinal dependence, particularly at high latitude, of day-night ratios.

Solutions for the transport processes are obtained from a mass-conserving, forward-time, space-centered finite difference formulation of the equations. The transport computations are further time split into those for vertical and horizontal advection and diffusion. A backward-time implicit formulation is used for the horizontal diffusion and a forward explicit formulation is used for all other transport processes. The calculations for advection are modified by a term M that improves the accuracy from first order to nearly second

order. This technique for improving the accuracy is practical because the velocities are prescribed and do not vary daily.

The differential and corresponding finite difference forms of the horizontal transport equations are as follows.

Advection (forward-time, space-centered, explicit):

$$\frac{\partial X}{\partial t} = -\frac{1}{R\cos\theta}\frac{\partial}{\partial\theta}(\cos\theta\, vX) \tag{17a}$$

$$X_{ij}^{k+1} = X_{ij}^{k} - \frac{1}{\cos\theta}\left(\frac{\Delta t}{2R\Delta\theta}\right)\left(\tilde{v}_{i+1,j}X_{i+1,j}^{k} - \tilde{v}_{i-1,j}X_{i-1,j}^{k}\right) \tag{17b}$$

where

$$X_{ij}^{k} = X(\theta_i, z_j, t_k)$$

$$\tilde{v}_{ij} = \cos\theta_i\, v(\theta_i, z_j)$$

Diffusion (forward-time, space-centered, implicit):

$$\frac{\partial X}{\partial t} = \frac{1}{\cos\theta}\frac{\partial}{R\partial\theta}\left(\cos\theta\left\{K_{yy}^{*}\frac{\partial X}{R\partial\theta} + K_{yz}\left[\frac{\partial X}{\partial z} + \left(\frac{1}{H} + \frac{1}{T}\frac{dT}{dz}\right)X\right]\right\}\right) \tag{18a}$$

$$\begin{aligned} X_{ij}^{k+1} = {} & X_{ij}^{k} + \frac{1}{\cos\theta_i}\frac{\Delta t}{2(R\Delta\theta)^2}\left[\left(\tilde{K}_{yy}^{*}{}_{i+1,j} + \tilde{K}_{yy}^{*}{}_{ij}\right)\left(X_{i+1,j}^{k+1} - X_{ij}^{k+1}\right)\right. \\ & \left. - \left(\tilde{K}_{yy}^{*}{}_{ij} + \tilde{K}_{yy}^{*}{}_{i-1,j}\right)\left(X_{ij}^{k+1} - X_{i-1,j}^{k+1}\right)\right] \\ & + \frac{1}{\cos\theta_i}\left(\frac{\Delta t}{4R\Delta\theta\Delta z}\right)\left[\tilde{K}_{yz}{}_{i+1,j}\left(X_{i+1,j+1}^{k} - X_{i+1,j-1}^{k}\right) - \tilde{K}_{yz}{}_{i-1,j}\left(X_{i-1,j+1}^{k}\right.\right. \\ & \left.\left. - X_{i-1,j-1}^{k}\right)\right] + \frac{1}{\cos\theta_i}\frac{\Delta t}{2R\Delta\theta}\left[(K_{yz}h_T)_{i+1,j}X_{i+1,j}^{k} - (\tilde{K}_{yz}h_T)_{i-1,j}X_{i-1,j}^{k}\right] \end{aligned} \tag{18b}$$

where

$$\tilde{K}_{yy}^{*} = \cos\theta_i\, K_{yy}^{*}(\theta_i, z_j)$$

$$K_{yy}^{*} = K_{yy} + M$$

$$\tilde{K}_{yz} = \cos\theta_i\, K_{yz}(\theta_i, z_j)$$

$$h_{T_{ij}} = \frac{1}{H_{ij}} + \frac{1}{T_{ij}} \frac{T_{i,j+1} - T_{i,j-1}}{2\Delta z}$$

$$M = \frac{\Delta t}{2} \max \left[v^2_{i-1,j-1}, v^2_{i-1,j}, v^2_{i-1,j+1}, v^2_{i,j-1}, v^2_{i,j}, \right.$$

$$\left. v^2_{i,j+1}, v^2_{i+1,j-1}, v^2_{i+1,j}, v^2_{i+1,j+1} \right]$$

Equations (18b) can be rewritten as a tridiagonal system and solved for X^{k+1}_{ij} by a standard inversion technique (e.g., Ames, ref. 18; also see Turco and Whitten, ref. 2).

The differential and corresponding finite difference forms of the vertical transport equations are as follows.

Advection (forward-time, space-centered, explicit):

$$\frac{\partial X}{\partial t} = - \frac{\partial}{\partial z} (wX) \tag{19a}$$

$$X^{k+1}_{i,j} = X^k_{i,j} - \left(\frac{\Delta t}{2\Delta z} \right) \left[w_{i,j+1} X^k_{i,j+1} - w_{i,j-1} X^k_{i,j-1} \right] \tag{19b}$$

Diffusion (forward-time, space-centered, explicit):

$$\frac{\partial X}{\partial t} = \frac{\partial}{\partial z} \left\{ K_{zz} \left[\frac{\partial X}{\partial z} + \left(\frac{1}{H} + \frac{1}{T} \frac{dT}{dz} \right) X \right] + K_{yz} \frac{1}{R} \frac{\partial X}{\partial \theta} \right\} \tag{20a}$$

$$X^{k+1}_{i,j} = X^k_{ij} + \frac{\Delta t}{2(\Delta z)^2} \left[\left(K_{\substack{zz \\ i,j+1}} + K_{\substack{zz \\ i,j}} \right) \left(X^k_{i,j+1} + X^k_{i,j} \right) \right.$$

$$- \left(K_{\substack{zz \\ ij}} + K_{\substack{zz \\ i,j-1}} \right) \left(X^k_{ij} + X^k_{i,j-1} \right) \Bigg] + \frac{\Delta t}{2\Delta z} \left[(K_{zz} h_T)_{i,j+1} X^k_{i,j+1} \right.$$

$$\left. - (K_{zz} h_T)_{i,j-1} X^k_{i,j-1} \right] + \frac{\Delta t}{4R\Delta\theta\Delta z} \left[K_{\substack{yz \\ i,j+1}} \left(X^k_{i+1,j+1} - X^k_{i-1,j+1} \right) \right.$$

$$\left. - K_{\substack{yz \\ i,j-1}} \left(X^k_{i+1,j-1} - X^k_{i-1,j-1} \right) \right] \tag{20b}$$

In our model we have chosen $\Delta\theta = 5°$ and $\Delta z = 2.5$ km. Because the formulas for the finite difference forms of the boundary condition are very lengthy, but not essential for immediate considerations, we present them in the appendix.

It is important to note that our differencing techniques for transport are mass-conserving. They are also quite accurate as we have verified with the aid of simple sinusoidal functions. There proved to be very little distortion or change in amplitude of the sinusoidal forms as a result of advective effects. A form of X with sinusoidal time and space dependence was inserted into the finite difference forms of the advective transport equations. Because the differential forms predict that such waves will not be distorted nor their amplitudes changed with time, we desire the same type of behavior for the finite difference solutions. Wave distortion and attenuation proved to be small.

Turco and Whitten (ref. 17) showed that in the stratosphere, diurnal averaging of the vertical transport terms in the continuity equations can be neglected. This is so because the time constants of species that experience large day-night variations are small compared to typical transport times. It is easily shown that similar considerations hold for the horizontal and "off-diagonal" transport. Hence we can neglect diurnal averaging in computing transport of species.

SOME RESULTS

The Ames two-dimensional model was used to study the distribution of various trace species (ozone, nitric acid, and carbon 14) in the stratosphere and to assess the effect on ozone of various pollutants. In this section we compare our predictions of ozone, nitric acid, and carbon 14 with measurement and show how our set of transport parameters is supported by observation.

Figure 4 shows some calculated profiles of ozone concentration for the midspring season together with measured data summarized by Wilcox et al. (ref. 19) for altitudes below 35 km; the high altitude data were obtained by polar-orbiting satellites (I. Eberstein, Goddard Space Flight Center, private communication). The topside concentrations (above 40 km), which are quite close to the measured values, are strongly dependent on the rate of ozone destruction by HO_x catalysis; OH concentrations in excess of 10^7 cm^{-3} are required to match the observed ozone profiles. At altitudes below 30 km, where ozone abundance is dominated by transport, our predicted profiles are quite close to those observed.

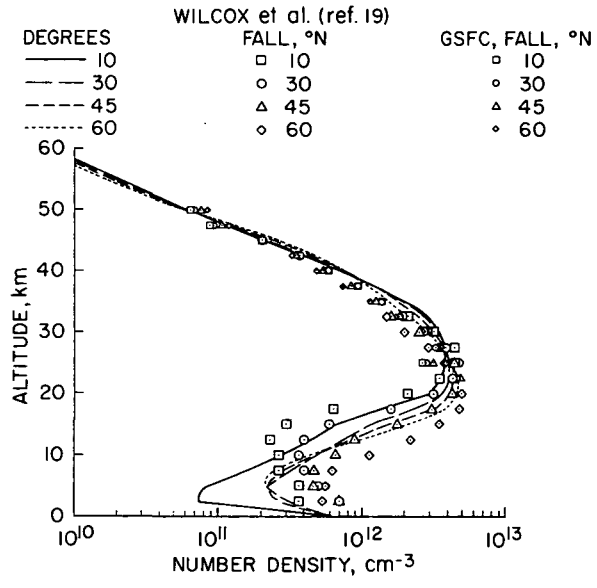

Figure 4.- Vertical distributions of ozone at various latitudes.

In comparing the predicted ozone abundance in the transport region with observed data it is instructive to employ the vertical

column density as a function of latitude. Transport parameters must, of course, be selected such that the predicted column densities are reasonably close to observed values. Louis (ref. 7) attempted to do this with the aid of a time-dependent model whose eddy diffusion coefficients were deduced from observed ozone distributions. Then his model was tested by simulating the distribution of radioactive debris from Chinese and American nuclear explosions. As one might expect, the agreement was very good because chemical production and loss of ozone was not included in the calculations used to deduce the K's from observed ozone distributions. In other words, ozone, like the radioactive debris, was treated as an inert tracer.

In order to check the effects when ozone chemistry is included, we have run our model (which includes photochemical production and loss terms) using Louis's transport parameters. The resulting ozone column density distribution (as a function of latitude), shown in figure 5, is obviously in strong disagreement with observation. However, when the same type of distribution is calculated with our set of transport parameters, the resulting column density distribution, shown in figure 6, is in very good agreement with observation. This emphasizes the need to take into account the complete chemistry, sources, and sinks of any tracer used to deduce transport parameters.

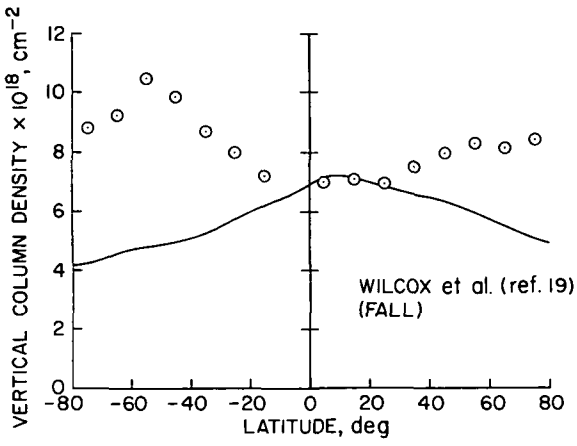

Figure 5.- Ozone column density as a function of latitude, using Louis' transport parameters.

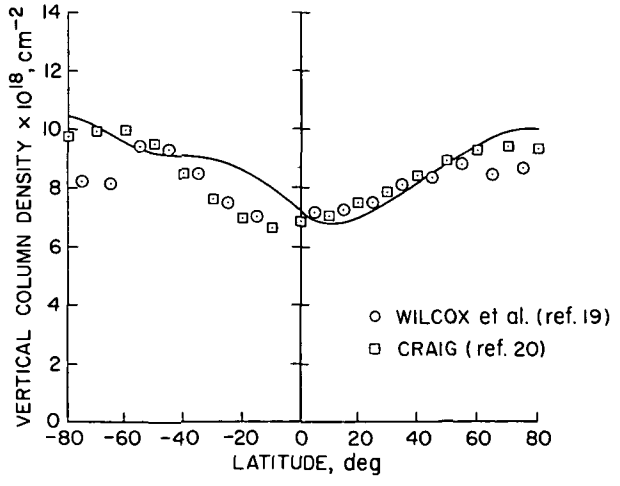

(a) Summer in the Northern Hemisphere.

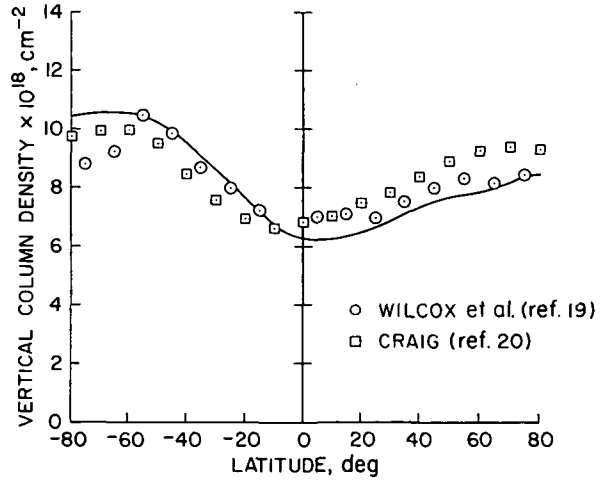

(b) Fall in the Northern Hemisphere.

Figure 6.- Ozone column density as a function of latitude; using our transport parameters.

Our predicted nitric acid column distribution for the same seasons is illustrated in figure 7. Since the chemistry of NO_x compounds differs from ozone chemistry, we expect the distributions to be different. In particular we expect HNO_3 column density latitudinal gradients to be larger than the corresponding ozone gradients because HNO_3 loss rates at all latitudes are smaller than those of ozone. This difference is both predicted and observed.

Finally, figure 8 compares the predicted and measured carbon 14 concentrations. Although the removal rate of C^{14} from the lower stratosphere appears to be somewhat too rapid, insistence on better agreement is probably not reasonable because the quality of the observed distributions at altitudes above 20 km is poor. We believe that we have found quite good overall agreement with the set of tracers (ozone, HNO_3, and carbon 14).

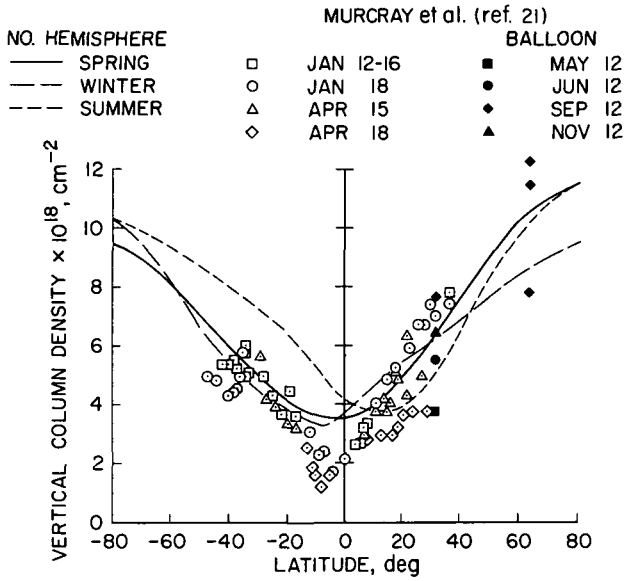

Figure 7.- Nitric acid column density as a function of latitude. Balloon measurements were made in 1970.

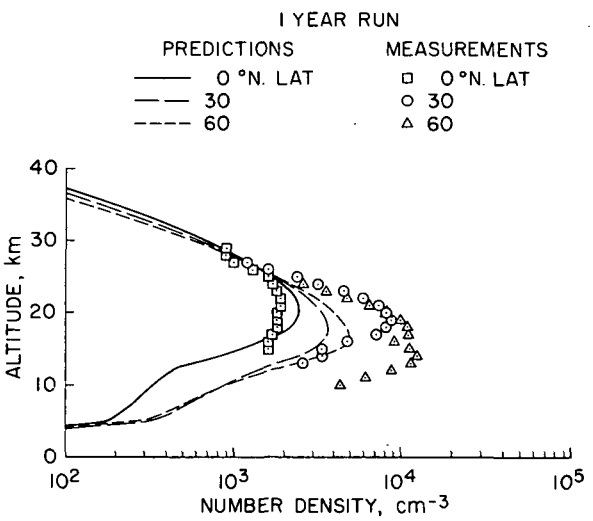

Figure 8.- Vertical distributions of carbon 14 at various latitudes. Experimental points are from Johnston et al. (ref. 22).

CONCLUSIONS

We have presented a complete and concise outline of our two-dimensional atmospheric computer simulation. Some of the unique aspects of our model are:

1. We are able to match simultaneously the observed distributions of several stratospheric tracers.

2. Our transport parameters are physically realistic.

3. We use an averaging scheme for simulating the effects of diurnal variations of atmospheric constituent concentrations.

4. We use an accurate computational technique for transport of species.

5. Our model is computationally efficient.

Ames Research Center
National Aeronautics and Space Administration
Moffett Field, California 94035, April 14, 1977

APPENDIX

BOUNDARY CONDITIONS

The finite difference forms of the transport equations for the boundary points are as follows.

Horizontal Advection

Boundary at 80° S — zero flux boundary condition:

$$X^{k+1}_{1,j} = X^{k}_{1,j} + \frac{\Delta t}{2\Delta y \cos \theta_1}\left[\tilde{v}_{2,j}X^{k}_{2,j} + \tilde{v}_{1,j}X^{k}_{1,j}\right]$$

Boundary at 80° N — zero flux boundary condition:

$$X^{k+1}_{N,j} = X^{k}_{Nj} + \frac{\Delta t}{2\Delta y \cos \theta_N}\left[\tilde{v}_{N-1,j}X^{k}_{N-1,j} + \tilde{v}_{Nj}X^{k}_{N,j}\right]$$

Horizontal Diffusion

Boundary at 80° S — zero flux boundary condition:

$$X^{k+1}_{1,j} = X^{k}_{1,j} + \frac{\Delta t}{2(\Delta y)^2 \cos \theta_1}\left(\tilde{K}_{\substack{yy \\ 2,j}} + \tilde{K}_{\substack{yy \\ 1,j}}\right)\left(X^{k+1}_{2,j} - X^{k+1}_{1,j}\right)$$

$$+ \frac{\Delta t}{4\Delta y \Delta z \cos \theta_1}\left[\tilde{K}_{\substack{yz \\ 2,j}}\left(X^{k}_{2,j+1} - X^{k}_{2,j-1}\right) + K_{\substack{yz \\ 1,j}}\left(X^{k}_{1,j+1} - X^{k}_{1,j-1}\right)\right]$$

$$+ \frac{\Delta t}{2\Delta y \cos \theta_1}\left[(\tilde{K}_{yz}h_T)_{2,j}X^{k}_{2,j} + (\tilde{K}_{yz}h_T)_{ij}X^{k}_{kj}\right]$$

Boundary at 80° N — zero flux boundary condition:

$$X^{k+1}_{N,j} = X^{k}_{N,j} - \frac{\Delta t}{2(\Delta y)^2 \cos \theta_N}\left(K_{\substack{yy \\ N,j}} + K_{\substack{yy \\ N-1,j}}\right)\left(X^{k+1}_{N,j} - X^{k+1}_{N-1,j}\right)$$

$$+ \frac{\Delta t}{4\Delta y \Delta z \cos \theta_N}\left[\tilde{K}_{\substack{yz \\ N-1,j}}\left(X^{k}_{N-1,j+1} - X^{k}_{N-1,j-1}\right) + \tilde{K}_{\substack{yz \\ N,j}}\left(X_{N,j+1} - X^{k}_{N,j-1}\right)\right]$$

$$+ \frac{\Delta t}{2\Delta y \cos \theta_N}\left[(\tilde{K}_{yz}h_T)_{N-1,j} + (\tilde{K}_{YZ}h_T)_{N,j}X^{k}_{N,j}\right]$$

Vertical Advection

Upper boundary ($j = M$) — zero flux boundary condition:

$$X_{i,M}^{k+1} = X_{iM}^{k} + \frac{\Delta t}{2\Delta z}\left(\omega_{iM} X_{iM}^{k} + \omega_{iM-1}^{k} X_{i,M-1}^{k}\right)$$

Lower boundary ($j = 1$) — specified density:

$X_{i,1}^{k+1}$ = density specified on chemical equilibrium

$X_{i,1}^{k+1}$ = value calculated from chemical equations or specified flux

(The specified flux could be added in the diffusion transport calculation — that is, modelled as a diffusion transport, or added in the advection transport, or added in the advection transport calculation. In this program, the specified flux is added in the diffusion transport calculation and the flux due to advection transport is set equal to zero.)

$$X_{i,1}^{k+1} = X_{i,1}^{k} - \frac{\Delta t}{\Delta z}\left(\omega_{i,1} X_{i,1}^{k} + \omega_{i,2}^{k} X_{i,2}^{k}\right)$$

Vertical Diffusion

Upper boundary ($j = M$) — zero flux boundary condition:

$$X_{i,M}^{k+1} = X_{iM}^{k} - \frac{\Delta t}{4\Delta y \Delta z}\left[K_{yz_{iM}}\left(X_{i+1,M}^{k} - X_{i-1,M}^{k}\right) + K_{yz_{i,M-1}}\left(X_{i+1,M-1}^{k} - X_{i-1,M-1}^{k}\right)\right]$$

$$- \frac{\Delta t}{2(\Delta z)^2}\left[\left(K_{zz_{iM}} + K_{zz_{iM-1}}\right)\left(X_{iM}^{k} - X_{iM-1}^{k}\right)\right]$$

$$- \frac{\Delta t}{2\Delta z}\left[\left(K_{zz} h_T\right)_{iM} X_{iM}^{k} + \left(K_{zz} h_T\right)_{iM-1} X_{iM-1}^{k}\right]$$

Lower boundary ($j = 1$) — specified density:

$X_{i,1}^{k+1}$ = density specified or chemical equilibrium.

$X_{i,1}^{k+1}$ = value calculated from chemical equations or specified flux.

$$X_{i,1}^{k+1} = X_{i,1}^{k} + 2\frac{\Delta t \phi_B}{\Delta z} + \frac{\Delta t}{2\Delta y \Delta z}\left[K_{\substack{yz \\ i1}}\left(X_{i+1,1}^{k} - X_{i-1,1}^{k}\right) + K_{\substack{yz \\ i,2}}\left(X_{i+1,2}^{k} - X_{i-1,2}^{k}\right)\right]$$

$$+ \frac{\Delta t}{(\Delta z)^2}\left[\left(K_{\substack{zz \\ i1}} + K_{\substack{zz \\ i2}}\right)\left(X_{i,2}^{k} - X_{i,1}^{k}\right)\right] + \frac{\Delta t}{\Delta z}\left[(K_{zz}h_T)_{i1}X_{i,1}^{k} + (K_{zz}h_T)_{i2}X_{i,2}^{k}\right]$$

where ϕ_B = flux specified at the lower boundary.

REFERENCES

1. Borucki, W. J.; Whitten, R. C.; Watson, V. R.; Woodard, H. T.; Riegel, C. A.; Capone, L. A.; and Becker, T.: Model Predictions of Latitude-Dependent Ozone Depletion Due to Supersonic Transport Operations. AIAA J. vol. 14, no. 12, 1976, pp. 1738-1745.

2. Turco, R. P.; and Whitten, Robert C.: The NASA Ames Research Center One- and Two-Dimensional Stratospheric Models. Part I: The One-Dimensional Model. NASA TP-1002, 1977.

3. Oort, A. H.; and Rasmussen, E. M.: Atmospheric Circulation Statistics. NOAA Paper 5, 1971.

4. Nastrom, G. D.; and Belmont, A. D.: Diurnal Stratospheric Tide in Meridional Wind, 30 to 60 km by Season and Monthly Mean Temperatures, 20 to 60 km, at 80° N to 0° N. NASA CR-137738, 1975.

5. Murgatroyd, R. J.; and Singleton, F.: Possible Meridional Circulations in the Stratosphere and Mesosphere. Quart. J. Roy. Met. Soc., vol. 87, no. 372, 1961, pp. 125-135.

6. Vincent, D. G.: Mean Meridional Circulations in the Northern Hemisphere Lower Stratosphere During 1964 and 1965. Quart. J. Roy. Meteor. Soc., vol. 94, no. 401, 1968, pp. 333-349.

7. Louis, J.-F.: A Two-Dimensional Transport Model of the Atmosphere. Ph.D. Thesis, 1974, Univ. of Colorado, 1974.

8. Newell, R. E.: The Circulation of the Upper Atmosphere. Scientific American, vol. 210, no. 3, 1964, pp. 62-74.

9. Wu, M. -F.: Trace Constituents in the Stratosphere. Annual Report ERT-P-393, U.S. Dept. of Transportation, 1973.

10. Howard, Philip H.; and Hanchett, Arnold: Chlorofluorocarbon Sources of Environmental Contamination. Science, vol. 189, no. 4198, 1975, pp. 217-219.

11. Turco, R. P.; and Whitten, R. C.: A Comparison of Several Computational Techniques for Solving Some Common Aeronomic Problems. J. Geophys. Res., vol. 79, no. 22, 1974, pp. 3179-3185.

12. Hudson, Robert D.; and Mahle, Stephen H.: Photodissociation Rates of Molecular Oxygen in the Mesosphere and Lower Thermosphere. J. Geophys Res., vol. 77, no. 16, 1972, pp. 2902-2914.

13. Shimazaki, T.; and Ogawa, T.: On the Theoretical Model of Vertical Distributions of Minor Neutral Constituent Concentrations in the Stratosphere. NOAA-TM-ERL-OD-20, Boulder, Colorado, 1974.

14. Shimazaki, T.; and Ogawa, T.: Theoretical Modeling of Minor Constituents Distribution in the Stratosphere and the Impact of SST Exhaust Gases. Proceedings of the International Association of Meteorology and Atmospheric Physics Conference, Melbourne, Australia, IAMPP Publication 15a, Toronto, 1974, pp. 1062-1075.

15. Shimazaki, Tatsuo; Ogawa, Tushiro; and Farrell, B. C.: Simplified Methods for Calculating Photodissociation Rates of Various Molecules in Schumann-Runge Band Systems in the Upper Atmosphere. NASA TN D-8399, 1977.

16. Cogley, Allen C.; and Borucki, William J.: Exponential Approximation for Daily Average Solar Heating or Photolysis. J. Atmos. Sci., vol. 33, 1976, pp. 1347-1356.

17. Turco, R. P.; and Whitten, Robert C.: A Note on the Diurnal Averaging of Aeronomic Models. J. Atmos. Terr. Phys., 1977. (To be published.)

18. Ames, William F.: Numerical Methods for Partial Differential Equations. Barnes and Noble, New York, 1969.

19. Wilcox, R. W.; Nastrom, G. D.; and Belmont, A. D.: Periodic Analysis of Total Ozone and Its Vertical Distribution. NASA CR-137737, 1975.

20. Craig, Richard A.: The Upper Atmosphere; Meteorology and Physics. Academic Press, New York, 1965.

21. Murcray, D. G.; Barker, D. B.; Brooks, J. N.; Goldman, A.; and Williams, W. J.: Seasonal and Latitudinal Variation of the Stratospheric Concentration of HNO_3. Geophys. Res. Lett., vol. 2, no. 6, 1975, pp. 223-225.

22. Johnston, Harold S.; Kattenborn, David; and Whitten, Gary: Use of Excess Carbon 14 Data to Calibrate Models of Stratospheric Ozone Depletion by Supersonic Transports. J. Geophys. Res., vol. 81, no. 3, 1976, pp. 368-380.

1. Report No.	2. Government Accession No.	3. Recipient's Catalog No.
NASA TP-1003		

4. Title and Subtitle	5. Report Date
THE NASA AMES RESEARCH CENTER ONE- AND TWO-DIMENSIONAL STRATOSPHERIC MODELS. PART II: THE TWO-DIMENSIONAL MODEL	September 1977
	6. Performing Organization Code

7. Author(s)	8. Performing Organization Report No.
R. C. Whitten,* W. J. Borucki,* V. R. Watson,* T. Shimazaki,* H. T. Woodward,* C. A. Riegel,† L. A. Capone,† and T. Becker‡	A-6982
	10. Work Unit No. 197-30-02

9. Performing Organization Name and Address	11. Contract or Grant No.
*Ames Research Center, Moffett Field, Calif. 94035 †Dept. of Meteorology, San Jose State Univ., San Jose, Calif. 95102 ‡Informatics, Inc., Palo Alto, Calif. 94303	

12. Sponsoring Agency Name and Address	13. Type of Report and Period Covered
National Aeronautics and Space Administration Washington, D. C. 20546	Technical Paper
	14. Sponsoring Agency Code

15. Supplementary Notes

16. Abstract

The Ames two-dimensional model of stratospheric trace constituents is presented in detail. The derivation of pertinent transport parameters and the numerical solution of the species continuity equations, including a technique for treating the "stiff" differential equations that represent the chemical kinetic terms, and appropriate methods for simulating the diurnal variations of the solar zenith angle and species concentrations are discussed. Predicted distributions of tracer constituents (ozone, carbon 14, nitric acid) are compared with observed distributions.

17. Key Words (Suggested by Author(s))	18. Distribution Statement
Stratosphere Atmospheric model Atmospheric photochemistry	Unlimited STAR Category - 47

19. Security Classif. (of this report)	20. Security Classif. (of this page)	21. No. of Pages	22. Price*
Unclassified	Unclassified	21	$3.25

*For sale by the National Technical Information Service, Springfield, Virginia 22161

NASA-Langley, 1977

National Aeronautics and
Space Administration

Washington, D.C.
20546

Official Business
Penalty for Private Use, $300

SPECIAL FOURTH CLASS MAIL
BOOK

Postage and Fees Paid
National Aeronautics and
Space Administration
NASA-451

U.S.MAIL

NASA

POSTMASTER: If Undeliverable (Section 158
Postal Manual) Do Not Return